**Atmospheric
Chemistry
and Physics**

Depositional ice nucleation onto crystalline hydrated NaCl particles: a new mechanism for ice formation in the troposphere

M. E. Wise[1,2]**, K. J. Baustian**[2,3]**, T. Koop**[4]**, M. A. Freedman**[5]**, E. J. Jensen**[6]**, and M. A. Tolbert**[1,2]

[1]Department of Chemistry & Biochemistry, University of Colorado, Boulder, CO 80309, USA
[2]Cooperative Institute for Research in Environmental Sciences, University of Colorado, Boulder, CO 80309, USA
[3]Department of Atmospheric and Oceanic Science, University of Colorado, Boulder, CO 80309, USA
[4]Faculty of Chemistry, Bielefeld University, 33615 Bielefeld, Germany
[5]Department of Chemistry, The Pennsylvania State University, University Park, PA 16802, USA
[6]NASA Ames Research Center, Moffett Field, CA, USA

Correspondence to: M. A. Tolbert (tolbert@colorado.edu), M. Wise (mawise@cu-portland.edu)

Abstract. Sea-salt aerosol (SSA) particles are ubiquitous in the marine boundary layer and over coastal areas. Therefore SSA have ability to directly and indirectly affect the Earth's radiation balance. The influence SSA have on climate is related to their water uptake and ice nucleation characteristics. In this study, optical microscopy coupled with Raman spectroscopy was used to detect the formation of a crystalline NaCl hydrate that could form under atmospheric conditions. $NaCl_{(s)}$ particles ($\sim$1 to 10 μm in diameter) deliquesced at 75.7 ± 2.5 % RH which agrees well with values previously established in the literature. $NaCl_{(aq)}$ particles effloresced to a mixture of hydrated and non-hydrated particles at temperatures between 236 and 252 K. The aqueous particles effloresced into the non-hydrated form at temperatures warmer than 252 K. At temperatures colder than 236 K all particles effloresced into the hydrated form. The deliquescence relative humidities (DRH) of hydrated $NaCl_{(s)}$ particles ranged from 76.6 to 93.2 % RH. Based on the measured DRH and efflorescence relative humidities (ERH), we estimate crystalline NaCl particles could be in the hydrated form 40–80 % of the time in the troposphere. Additionally, the ice nucleating abilities of $NaCl_{(s)}$ and hydrated $NaCl_{(s)}$ were determined at temperatures ranging from 221 to 238 K. Here, depositional ice nucleation is defined as the onset of ice nucleation and represents the conditions at which the first particle on the substrate nucleated ice. Thus the values reported here represent the lower limit of depositional ice nucleation. $NaCl_{(s)}$ particles depositionally nucleated ice at an average S_{ice} value of 1.11 ± 0.07. Hydrated $NaCl_{(s)}$ particles depositionally nucleated ice at an average S_{ice} value of 1.02 ± 0.04. When a mixture of hydrated and anhydrous $NaCl_{(s)}$ particles was present in the same sample, ice preferentially nucleated on the hydrated particles 100 % of the time. While both types of particles are efficient ice nuclei, hydrated $NaCl_{(s)}$ particles are better ice nuclei than $NaCl_{(s)}$ particles.

1 Introduction

It is known that sea-salt aerosol (SSA) particles are ubiquitous in the marine boundary layer and over coastal areas. These particles are injected into the atmosphere due to wind and wave action over oceans. It is estimated that approximately 17 Tg of SSA particles enter the atmosphere per year (Textor et al., 2006). Of this amount 15 % is emitted as submicron size particles. Therefore it is appropriate that studies have been carried out to estimate the radiative effects of SSA particles. Haywood et al. (1999) estimated the direct radiative effect of SSA particles to be -1.5 W m^{-2} to -5 W m^{-2}. Vinoj and Satheesh (2003) estimated the indirect radiative effect arising from the CCN activity of SSA over the Indian Ocean to be -7 ± 4 W m^{-2}.

SSA particles are made up of many different chemical compounds. The ionic composition of dry, freshly emitted SSA can be inferred from the composition of natural seawater. Natural seawater contains 55.40 % (w/w) Cl$^-$, 30.61 % Na$^+$, 7.68 % SO$_4^{2-}$ and 3.69 % Mg^{2+} (Pilson, 1998). It is also known that natural SSA contains on the order of 10 % (w/w) organic compounds (Middlebrook et al., 1998). O'Dowd et al. (2004) found that SSA can be enriched in organic material relative to bulk seawater. This enrichment increases with decreasing particle size. Once emitted into

the atmosphere, SSA composition can change due to heterogeneous reactions in the atmosphere. For example, nitric acid can react with SSA to form gaseous hydrogen chloride and (depending on atmospheric conditions) aqueous or solid sodium nitrate (i.e., De Haan and Finlayson-Pitts, 1997)

Although natural SSA are chemically complex (which can affect water uptake properties) NaCl has been widely used as a proxy for SSA. The use of NaCl as a proxy for SSA is appropriate because many of the physical properties of SSA are controlled by NaCl. For example, Tang et al. (1997) found that for a specific dry particle size distribution, NaCl aerosol scattered light as efficiently as freshly formed sea salt aerosol (per unit mass). Therefore, several studies have been conducted to determine the conditions under which NaCl particles take up water to form solution droplets (deliquescence) and lose water to reform crystalline NaCl particles (efflorescence). It is widely accepted that, at room temperature, pure NaCl particles deliquesce at approximately 75 % relative humidity (DRH) and effloresce at approximately 45 % relative humidity (ERH) (i.e., Cziczo and Abbatt, 2000; Koop et al., 2000; Tang et al., 1977; Wise et al., 2005). Additionally, using a flow-tube apparatus, Cziczo and Abbatt (2000) found that the DRH and ERH of NaCl particles did not change substantially when temperature was decreased from 298 to 253 K. Koop et al. (2000) extended the temperature range at which the DRH and ERH of NaCl particles were determined using differential scanning calorimetry (DSC) measurements and flow cell microscopy. In agreement with Cziczo and Abbatt (2000), Koop et al. (2000) found that the DRH of NaCl particles did not change substantially at temperatures as low as 239 K.

Because NaCl is a ubiquitous tropospheric particle, it is important to elucidate the behavior of NaCl particles at even lower temperatures found throughout the troposphere. According to the NaCl phase diagram (Linke, 1965), at maximum NaCl solubility, a brine solution and the crystalline dihydrate form of NaCl ($NaCl \cdot 2H_2O_{(s)}$) are stable from 273 K to the eutectic temperature of 252 K. At temperatures below 252 K, solid ice and $NaCl \cdot 2H_2O_{(s)}$ (sodium chloride dihydrate) are stable. Cziczo and Abbatt (2000) did not find indications of $NaCl \cdot 2H_2O_{(s)}$ formation (at conditions predicted by the bulk phase diagram) during their NaCl water uptake experiments. Similarly Koop et al. (2000) did not find indications of $NaCl \cdot 2H_2O_{(s)}$ formation in their low temperature flow cell experiments because the DRH of the solid particles did not agree with the predicted DRH for $NaCl \cdot 2H_2O_{(s)}$. However, Koop et al. (2000) did find indications of $NaCl \cdot 2H_2O_{(s)}$ in their DSC experiments which was attributed to heterogeneous nucleation on available ice surfaces after ice formation. Krepelova et al. (2010) studied the surface of $NaCl/H_2O$ mixtures at temperatures warmer, including and colder than the eutectic temperature. Depending on temperature of the frozen solution, the surface could consist of ice, $NaCl \cdot 2H_2O_{(s)}$, and surface adsorbed water.

Cziczo et al. (2004) performed an in situ investigation of the chemical composition of anvil cirrus cloud residue near the Florida peninsula. They found that 26 % of the ice residue in the Florida area was sea salt. Cziczo et al. (2004) encountered cirrus clouds that appeared to incorporate both heterogeneous and homogeneous ice nucleation simultaneously. They inferred that sea salt likely nucleated ice via a homogeneous freezing mechanism and that insoluble particles (such as mineral dust) nucleated ice via a heterogeneous freezing mechanism. This inference was made due to the observation that sea salt particles dominated the larger size mode. However, it is possible that ice nucleated on hydrated $NaCl_{(s)}$ particles which would also be larger than anhydrous NaCl.

In the present study we re-examine NaCl deliquescence, efflorescence and ice nucleation at low temperatures. We use a combination of optical microscopy and Raman spectroscopy to probe the phase transitions and ice nucleating efficiency of sodium chloride particles under a range of tropospheric conditions. Specifically, this combination of techniques allows the visual and spectroscopic determination of the conditions at which micron-sized $NaCl_{(s)}$, $NaCl_{(aq)}$, and hydrated $NaCl_{(s)}$ particles are metastable or stable at tropospheric temperature conditions. It also allows a comparison of the depositional ice nucleating ability of $NaCl_{(s)}$ and hydrated $NaCl_{(s)}$.

2   Experimental

A Nicolet Almega XR Dispersive Raman spectrometer outfitted with a modified Linkham THMS600 environmental cell, a Buck Research Instruments CR-1A chilled mirror hygrometer, and a Linkham automated temperature controller was used to study deliquescence, efflorescence and depositional ice nucleation using pure $NaCl_{(s)}$ and hydrated $NaCl_{(s)}$ particles. The Raman spectrometer was equipped with an Olympus BX51 research-grade optical microscope which had the capability to magnify particles 10X, 20X, 50X and 100X. The experimental setup and procedure is similar to that used in Baustian et al. (2010) and Wise et al. (2010). Additional details are provided when the current experiment differs from that of Baustian et al. (2010) and Wise et al. (2010).

NaCl particles were generated by feeding a 10 wt % NaCl (Fisher Scientific, 99.9 % purity) solution at 2 ml min⁻¹ into an atomizer (TSI 3076) using a Harvard apparatus syringe pump. Pre-purified nitrogen gas at a flow rate of 3000 ccm was used to operate the atomizer. The particles exiting the atomizer were then impacted onto a hydrophobic quartz disc (silanized with RainX prior to experimentation) for analysis. Each data point presented in this manuscript represents an independently generated sample, i.e. in total about 150 samples were investigated. The diameters of the particles studied ranged from approximately 1 to 10 μm with typical values close to 5 μm.

2.1 Deliquescence and efflorescence of NaCl$_{(s)}$ and hydrated NaCl$_{(s)}$ particles

To begin a water uptake experiment, the silanized quartz disc containing NaCl$_{(s)}$ particles was placed inside the environmental cell at room temperature. The cell was sealed and water vapor was purged from the cell using a flow of ultra-high purity nitrogen. Once the frost point in the environmental cell reached approximately 213 K, the temperature of the particles was lowered to between 233 and 258 K using a combination of liquid nitrogen cooling and resistive heating. After the temperature of the particles equilibrated, water vapor was introduced into the cell until deliquescence was visually observed at 50X magnification. Raman spectra of the particles were then taken for verification. The focal point of the Raman laser can be adjusted. Thus, spectra representative of the chemical constituents contained throughout the depth of the particle can be obtained. Frost point measurements (error ±0.15 K) from the hygrometer allow determination of the water partial pressure within the cell. The sample (particle) temperature is measured using a platinum resistance sensor embedded in the sample block. Temperature calibrations are performed as described in Baustian et al. (2010). The average error in the temperature calibration is ±0.2 K for all experiments. The water partial pressure and sample temperature are used together to determine the RH during experimentation. The uncertainty in water partial pressure and temperature corresponds to an error of less than ±5 % RH over the range of experimental conditions studied. During experimentation, the rate of RH change ranged from 1–10 % RH per minute.

After deliquescence, water vapor was removed from the cell until efflorescence of all particles was observed. As with the deliquescence phase transition, efflorescence was monitored both visually and spectroscopically. Depending on particle temperature, either NaCl$_{(s)}$, hydrated NaCl$_{(s)}$ or a mixture of the two solid forms nucleated when the particles effloresced. If hydrated NaCl$_{(s)}$ formation was observed, the particles were subjected to a second RH cycle to determine the DRH and ERH of the hydrated particles. After each particle effloresced following the second RH cycle, Raman spectra of 50 different particles were collected to determine the percentage of solid particles that were anhydrous NaCl$_{(s)}$. In order to eliminate operator bias, 50 random particles were studied. Specifically, the substrate was moved in a straight line and each particle that was illuminated by the Raman laser was studied.

2.2 Depositional ice nucleation on NaCl$_{(s)}$ and hydrated NaCl$_{(s)}$ particles

To begin a depositional ice nucleation experiment on NaCl$_{(s)}$ particles, a quartz disc containing NaCl$_{(s)}$ particles was placed inside the environmental cell at room temperature. The cell was sealed, water vapor purged and the tempera-

ture of the particles was lowered to between 221 and 238 K. Water vapor was introduced into the cell continuously until ice nucleation was visually observed (at 10X magnification) and S_{ice} was recorded. The uncertainty in water partial pressure and temperature corresponds to an error in S_{ice} of less than 0.05 over the range of experimental conditions studied. Ice was confirmed using Raman spectroscopy. After the confirmation of ice, the water vapor was shut off and the ice was sublimed. A Raman spectrum of the ice nuclei (IN) was taken.

Depositional ice nucleation on a sample containing both NaCl$_{(s)}$ and hydrated NaCl$_{(s)}$ particles was also studied. Hydrated NaCl$_{(s)}$ could not be made at room temperature. Therefore, the experiment was initiated by deliquescing NaCl$_{(s)}$ and then efflorescing the particles at approximately 239 K. This was accomplished using the deliquescence/efflorescence procedure described above. A temperature of 239 K was chosen because it was experimentally determined that (after efflorescence) the majority of the particles were hydrated NaCl$_{(s)}$. However, some anhydrous NaCl$_{(s)}$ particles also formed. After the formation of the hydrated particles, the temperature of the particles was lowered to between 221 and 238 K at a rate of 2 K min^{-1}. As the temperature of the particles decreased from 239 K, it was important to maintain the RH in the environmental cell at values between 25 and 45 %. This RH range was chosen because at low RH values (6–25 %), the hydrated NaCl particles reverted to the anhydrous form and at high RH values (75 %) the anhydrous particles deliquesced. Furthermore, the cooling rate of 2 K/min was chosen so that an S_{ice} of greater than 1 was not attained before the desired temperature was reached. Once the solid particles reached the desired temperature, water vapor was introduced into the cell until ice nucleation was visually observed (at 10X magnification). Ice was confirmed using Raman spectroscopy. After the confirmation of ice, the water vapor was shut off and the ice was sublimed. A Raman spectrum of the IN was taken.

3 Results

Figure 1 presents images of NaCl particles (at 50X magnification) recorded from the optical microscope as RH was cycled from 0 to 76 % at 244 K. At 0.9 % RH, all of the particles on the quartz disc were NaCl$_{(s)}$. As RH was increased to 69.0 %, the morphology of the particles did not change and no water uptake was observed. At 69.0 % RH, the solid NaCl particles visually took up a small amount of water. The presence of water on particle (a) in Fig. 1 was confirmed using Raman spectroscopy. The spectrum is recorded in Fig. 2. Although subtle, the Raman signal due to water uptake is seen as a small increase in intensity over the broad range of 3000 to 3700 cm^{-1}. The DRH of NaCl$_{(s)}$ particles is extrapolated from higher temperature data (Tang and Munkelwitz, 1993 and Koop et al., 2000) and is ∼76.7 % RH at 244 K.
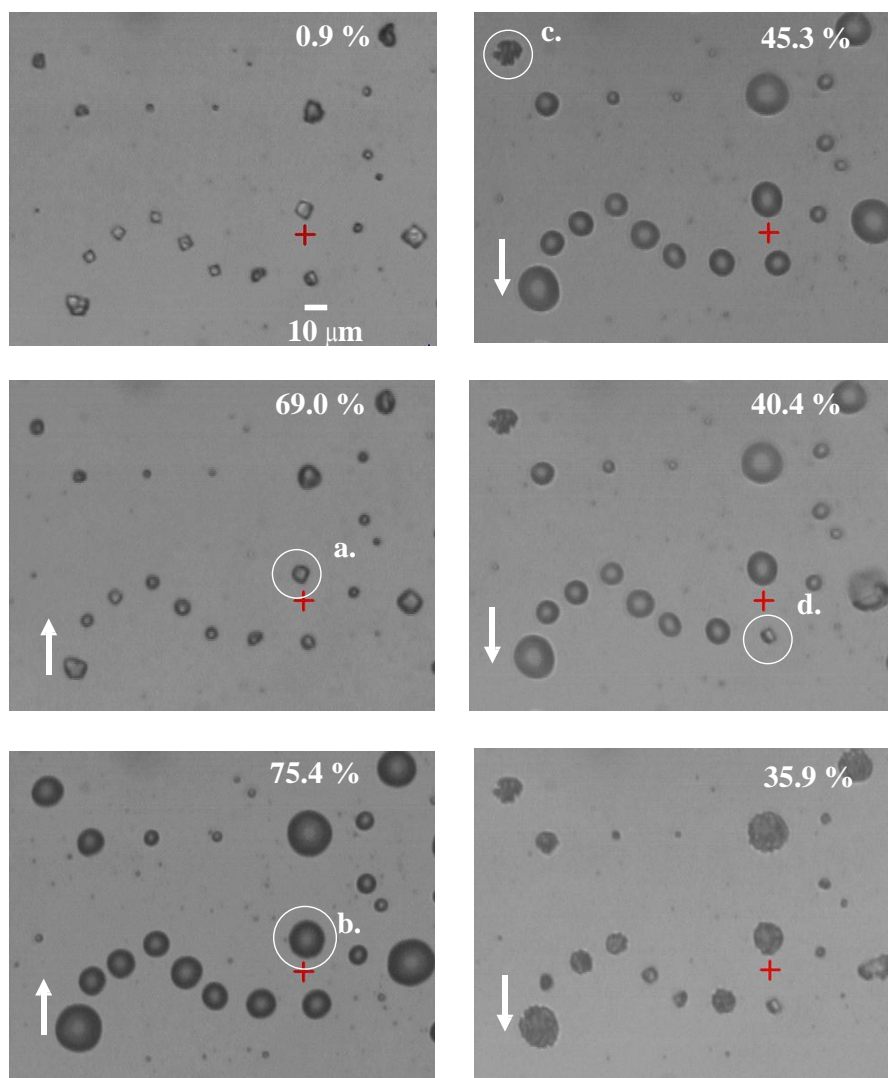
Fig. 1. NaCl particles at 244 K as RH is cycled. The up arrows indicate increasing water vapor in the environmental cell and the down arrows indicate decreasing water vapor in the environmental cell. The letters highlighting specific particles in Fig. 1 correspond to the letters denoting specific Raman spectra in Fig. 2. The red crosshairs, which indicate where the Raman laser is aimed, were moved so that the particles could be seen more easily.

This value is higher than the RH observed here for the on-set of water uptake. However, the NaCl$_{(s)}$ particles at 69.0 % were not fully dissolved. At this point, if the water vapor in the environmental cell were reduced, the particles would revert to their fully crystalline state. Slight water uptake prior to deliquescence was also observed on ammonium sulfate particles using Raman microscopy (Wise et al., 2010) and a variety of other soluble salt compounds using an environmental transmission electron microscope (Wise et al., 2008). Similar water uptake below the bulk DRH was also observed for other particles using H-TDMA and may be interpreted as water absorption into polycrystalline particles owing to capillary effects (Mikhailov et al., 2009). While the NaCl particles don't appear polycrystalline, perhaps microscopic

cracks or fissures could cause similar water uptake. Furthermore, Ewing (2005) showed that at water vapor pressures of ∼20 mbar at 24 °C (67 % RH), water adsorbs to the surfaces of NaCl crystallites with a surface coverage of ∼4.5 monolayers (see Fig. 9 of Ewing 2005). At 75.4 % RH, the NaCl$_{(s)}$ particles deliquesced in our experiment shown in Fig. 1. Deliquescence resulted in a notable increase in the Raman intensity between 3000 to 3700 cm^{-1} (Fig. 2b) and was visually confirmed by noting the RH at which the NaCl$_{(s)}$ core disappeared. The DRH of the NaCl$_{(s)}$ particles found in this experiment agrees well with the accepted value for NaCl$_{(s)}$.

After deliquescence, the RH in the environmental cell was decreased to 45.3 % RH and the particles gradually lost water resulting in decreasing size. At 45.3 % RH, one of the
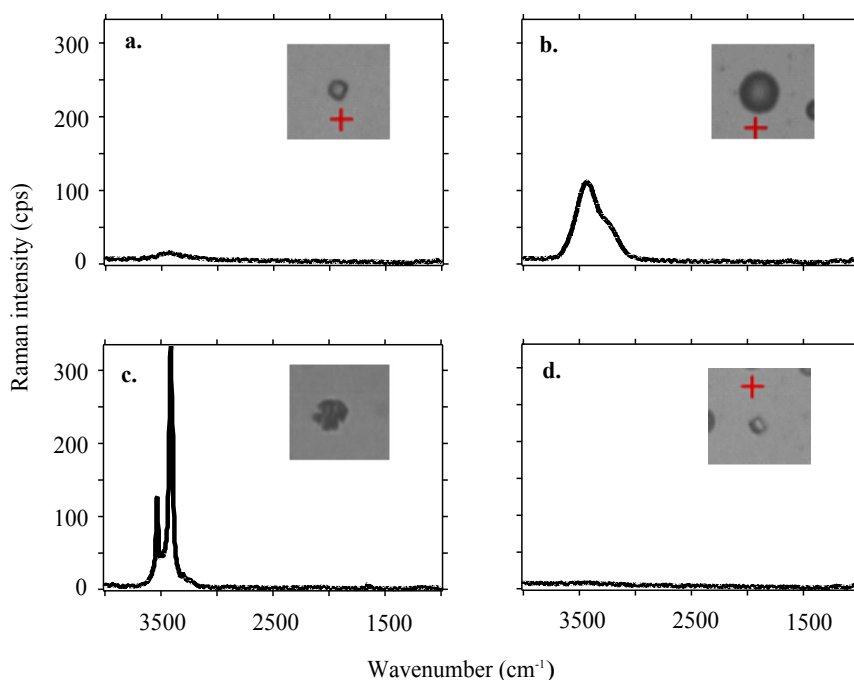
Fig. 2. Raman spectra of the particles highlighted in Fig. 1.

particles in the field of view effloresced (particle c). This particle did not effloresce into morphology consistent with that of NaCl$_{(s)}$. Particle (c) appeared round and bumpy whereas NaCl$_{(s)}$ particles appeared cubic. The Raman spectrum taken of particle (c) is included in Fig. 2. The spectrum has sharp Raman intensities at approximately 3530 cm^{-1} and 3410 cm^{-1}. The Raman spectrum of particle (c) is markedly different than that of NaCl$_{(s)}$ because NaCl$_{(s)}$ shows no features in this region. As the RH in the environmental cell decreased to 40.4 %, a cubic NaCl$_{(s)}$ particle formed (particle d). The Raman spectrum shown in Fig. 2 confirms that the particle is NaCl$_{(s)}$ due to the lack of peaks in the spectrum. When the RH decreased further to 35.9 % RH (Fig. 1), all the particles reverted to their solid form. In this particular experiment, the efflorescence of NaCl$_{(aq)}$ droplets occurred over a range of 35.9 to 45.3 % RH. The range of ERH values is not surprising given the stochastic nature of efflorescence and lies within the range of previously observed values (43–50 % RH; Martin, 2000). Further, particle size does not appear to affect the ERH. Similarly, Wise et al. (2005) observed this phenomenon with various salts (0.1–4 μm diameter) using a transmission electron microscope with an environmental cell.

From the water uptake experiment described above, it is apparent that two different forms of solid NaCl effloresced at 244 K. According to the bulk NaCl phase diagram (Linke, 1965), aqueous NaCl droplets are not stable at 244 K. Depending on the wt % of NaCl, a mixture of NaCl$_{(s)}$ and NaCl·2H$_2$O$_{(s)}$ is predicted to be present. Therefore, in the current experiment, the aqueous droplets that nucleated solid

particles between 36 and 45 % RH were in a metastable state prior to efflorescence. This result is not surprising as it is well known that micron-sized aqueous droplets significantly supercool and supersaturate before crystalline phases (salt or ice) nucleate homogeneously (Martin, 2000; Koop, 2004).

A question arises concerning the identity of the second form of solid NaCl. The logical choice for the identity of the solid is NaCl·2H$_2$O due to its presence in the bulk NaCl phase diagram. Dubessy et al. (1982) used the Raman microprobe MOLE to collect the Raman spectrum of a hydrated crystalline form of NaCl$_{(s)}$, supposedly NaCl·2H$_2$O$_{(s)}$, at 103 K. The Raman spectrum collected by Dubessy et al. (1982) had 8 sharp peaks. The positions of those peaks are highlighted with solid lines on a Raman spectrum of the non-cubic form of NaCl$_{(s)}$ (collected in this experiment at 244 K) in Fig. 3a. The Raman spectrum collected at 244 K did not have 8 distinct peaks; however, the peaks from the Dubessy et al. (1982) spectrum line up well with the peaks that are present. Perhaps the differences between the Dubessy et al. (1982) spectrum of NaCl·2H$_2$O$_{(s)}$ and the spectrum collected here is not due to a difference in composition but to differences in the temperatures at which the spectra were collected (103 K versus 244 K). To check this, the temperature of the particles was lowered to the minimum temperature attainable in the environmental cell (163 K). The Raman spectrum of the non-cubic form of NaCl$_{(s)}$ collected at 163 K is shown in Fig. 3b. Two peaks at ∼3209 cm^{-1} and 3089 cm^{-1} appeared in the Raman spectrum when the temperature was lowered to 163 K. These peaks match well
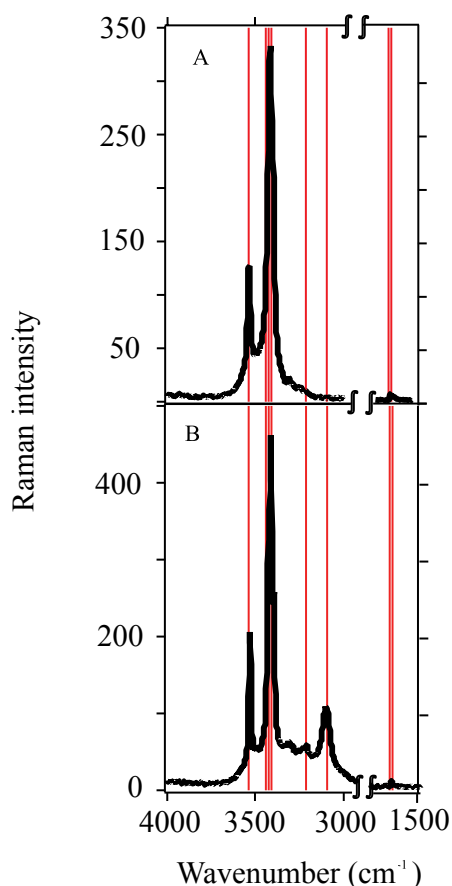
Fig. 3. (**A**) Raman spectrum of the non-cubic form of solid NaCl collected at 244 K. (**B**) Raman spectrum of the non-cubic form of solid NaCl collected at 163 K. The solid vertical lines highlight the peaks in the Raman spectrum collected by Dubessy et al. (1982) supposedly for solid sodium chloride dihydrate. The middle portion of the Raman spectrum has been removed because no peaks are present.

with the peaks in the spectrum of $NaCl \cdot 2H_2O_{(s)}$ collected by Dubessy et al. (1982) at 103 K. Therefore, the non-spherical, solid particles present in Fig. 1 definitively contain water and are possibly $NaCl \cdot 2H_2O_{(s)}$.

Assuming that particle size does not affect thermodynamics, the DRH of $NaCl_{(s)}$ should correspond to its solubility line in the bulk phase diagram. This is expected because particle size has been shown to affect ERH and DRH only below 100 nm in diameter (Biskos et al., 2006). Since the particles used in this experiment are significantly greater than 100 nm, the DRH of $NaCl_{(s)}$ and $NaCl \cdot 2H_2O_{(s)}$ should be predicted well using the bulk phase diagram. In order to test this prediction, a second water uptake experiment was conducted on a sample of mixed $NaCl_{(s)}$ and hydrated $NaCl_{(s)}$ particles. The results of a typical water uptake experiment with a sample of mixed phase particles are shown in Fig. 4. This water uptake experiment was a continuation of the water uptake ex-

periment performed at 244 K shown in Fig. 1. Therefore all the particles are the same.

At RH values less than 76.3 % all of the particles were solid but some were hydrated and some were anhydrous. As the RH in the environmental cell was increased to 76.3 %, the $NaCl_{(s)}$ particles deliquesced (see circled particle) and the hydrated $NaCl_{(s)}$ (see particle in the square) particles remained in the solid phase. A DRH of 76.3 % for $NaCl_{(s)}$ particles is consistent with the theoretical DRH for $NaCl_{(s)}$ particles at this temperature. There is a slight difference in DRH for the $NaCl_{(s)}$ particles shown in Fig. 4 compared to the particles shown in Fig. 1. This difference is due to normal experimental variation in the obtained DRH values. When the RH was increased to 89.6 % RH, the hydrated $NaCl_{(s)}$ particles deliquesced. Once all the particles deliquesced, water vapor was removed from the environmental cell until all the particles effloresced. All particles effloresced by 32.5 % RH. Interestingly, some of the particles effloresced into a phase that they did not originally start in. For example, the particle highlighted with the box started the RH cycle as a hydrated particle and finished the RH cycle as an anhydrous particle. The water in the crystal lattice of the hydrated $NaCl_{(s)}$ particles were removed when the RH in the environmental cell was dropped to 19.8 %. This transformation was accompanied by the cracking of the particle and the disappearance of all peaks in the Raman spectrum. The cracking phenomenon, which is the physical separation of a particle into multiple pieces, is evident in the last panel of Fig. 4. A similar behavior of a hydrated crystalline solid losing hydration water to form a less hydrated or dry crystalline form has also been observed in single aerosol particles consisting of LiI (Kurtz and Richardson, 1984).

Figure 5 shows the NaCl phase diagram adapted from Koop et al. (2000) in temperature/RH space rather than temperature/wt % space. Koop et al. (2000) described the construction of the phase diagram; therefore, only descriptions of the symbols are given here. The thick solid vertical line represents the accepted DRH values for $NaCl_{(s)}$ particles and the thick dotted vertical line represents the accepted ERH values for $NaCl_{(aq)}$ particles. These values are based on experimental measurements between 278 and 308 K (Tang and Munkelwitz, 1993). The thin lines extending from the accepted DRH and ERH lines are extrapolations to lower temperatures. The open diamonds and crosses represent the DRH and ERH of the NaCl particles studied here at temperatures between 233 and 256 K. All DRH and ERH data were put into bins that span two degrees Kelvin and averaged. Each data point represents the average value for each temperature bin. The error range is the high and low value for each bin. The DRH of $NaCl_{(s)}$ and the ERH of $NaCl_{(aq)}$ particles measured here agree well with the extrapolated values of DRH and ERH. Furthermore, the measurements agree with the DRH (filled circles) and ERH (filled squares) observed by Koop et al. (2000) using a flow cell apparatus.
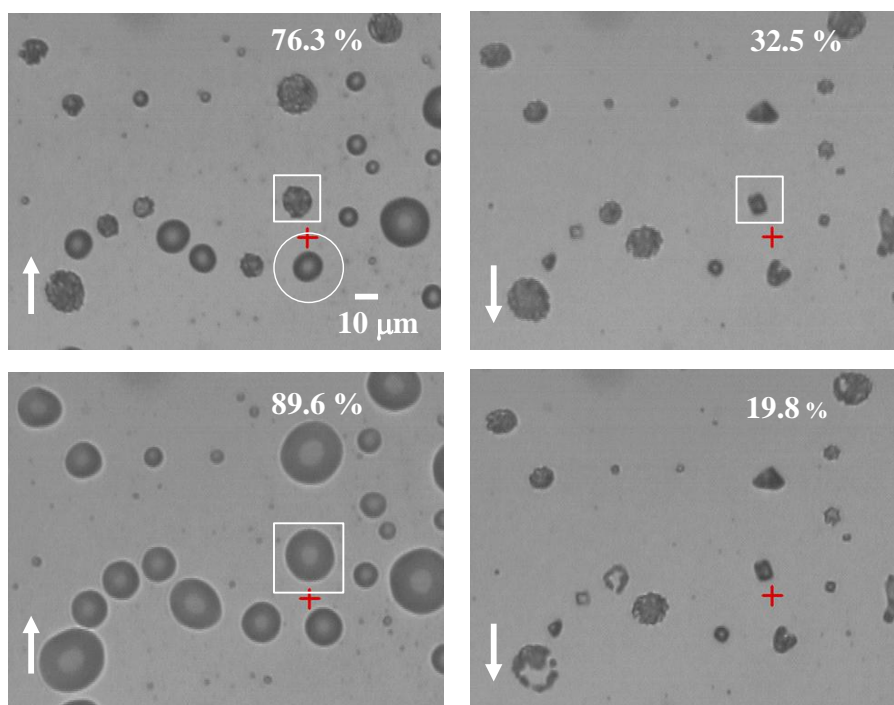
Fig. 4. NaCl particles (at 50X magnification) at 244 K as RH is cycled a second time. The up arrows indicate that water is being added to the environmental cell and the down arrows indicate that water is being removed from the environmental cell.
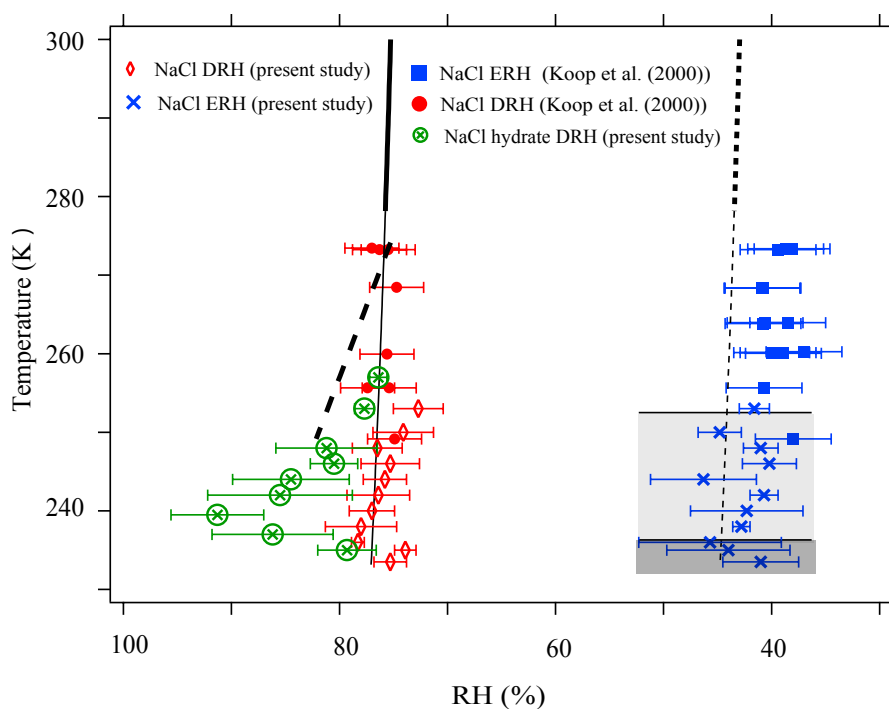

Fig. 5. NaCl phase diagram adapted from Koop et al. (2000): NaCl ERH (solid blue squares), NaCl DRH (solid red circles), high temperature NaCl DRH (solid black vertical line), high temperature NaCl ERH (dotted black vertical line), theoretical NaCl hydrate DRH (thick black dashed line). Data collected from the present study: NaCl hydrate DRH (crossed green circles), NaCl DRH (open red diamonds), NaCl ERH (blue crosses), region where mixed particles effloresce (light gray shade), region where hydrated particles effloresce (dark gray shade).
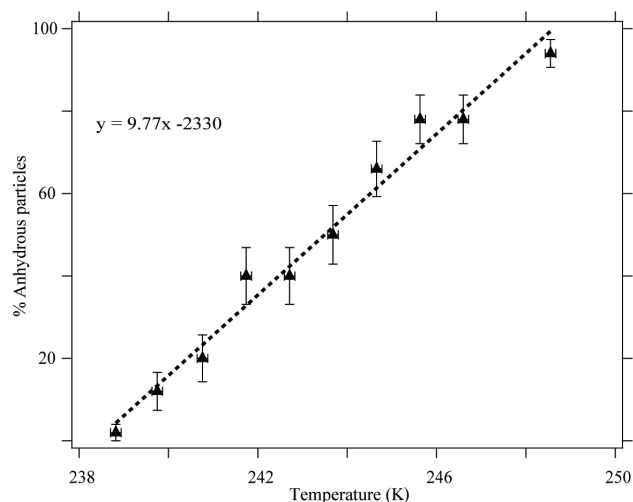
Fig. 6. Percent anhydrous particles versus temperature (K).

Using a flow tube apparatus at temperatures between 253 and 283 K, Cziczo and Abbatt (2000) also studied the water uptake properties of NaCl particles. The DRH and ERH measurements made by Cziczo et al. (2000) also agree with the measurements made here.

It was shown above (Fig. 1) that at 244 K a mixture of $NaCl_{(s)}$ and hydrated $NaCl_{(s)}$ particles form upon efflorescence of solution droplets. It was found that at temperatures warmer than 252 K, no hydrated $NaCl_{(s)}$ particles formed upon efflorescence. However, at temperatures between 236 and 252 K, a mixture of hydrated and anhydrous particles effloresced. The temperature region in which both hydrated and anhydrous particles nucleated is denoted with light gray shading in Fig. 5. Efflorescence experiments performed at temperatures colder than 236 K produced only hydrated $NaCl_{(s)}$. This temperature region is denoted with darker gray shading in Fig. 5. Because a mixture of hydrated and anhydrous particles formed between 236 and 252 K, efflorescence experiments were conducted to find the relationship between particle temperature and the percentage of particles in the anhydrous form. The results of these experiments are shown in Fig. 6. Between 239 and 249 K, there is a linear relationship between the temperature of the particles at efflorescence and the percentage of anhydrous $NaCl_{(s)}$ particles formed. Each data point utilizes 50 different particles and the error bars for each point represent the standard error assuming random sampling.

Although hydrated particles form between 236 and 239 K, the linear relationship between temperature and the percentage of anhydrous $NaCl_{(s)}$ particles formed breaks down. Similarly, between 249 and 252 K, the linear relationship is not valid. Therefore, between 239 and 249 K, the percentage of anhydrous $NaCl_{(s)}$ particles can be predicted if particle temperature is known.

Water uptake experiments were performed on hydrated $NaCl_{(s)}$ particles at temperatures between 235 and 247 K to determine their DRH. The results of these experiments are denoted with green crossed circles in Fig. 5. As before, the DRH data were put into bins that span two degrees Kelvin and averaged. The DRH of the hydrated particles found in this study do not agree well with the theoretical DRH of $NaCl \cdot 2H_2O_{(s)}$ (thick dashed line). However, the experimental points are scattered around a value of 87 % RH. This value is close to where $NaCl \cdot 2H_2O_{(s)}$ would deliquesce at 240 K (~85 % RH; Koop et al., 2000). However, the scatter in the DRH data for $NaCl \cdot 2H_2O_{(s)}$ is large when compared to the scatter for $NaCl_{(s)}$ DRH. Therefore, we cannot definitively confirm the identity of the hydrate. Additional water uptake experiments were performed on samples containing only hydrated particles. The DRH values determined in these experiments agreed well with the DRH values found in the mixed particle experiments. The question then remains as to why the hydrated particles do not deliquesce at the RH predicted for $NaCl \cdot 2H_2O_{(s)}$.

We cannot exclude the formation of another type of hydrate that has not been observed previously in the literature. While this could explain why the observed DRH values are different from those predicted for the dihydrate from bulk data, it appears to be inconsistent with the spectroscopic data. However, whether the hydrate observed in our experiments is identical to the dihydrate observed in bulk experiments, or is a metastable form of the dihydrate, or is yet another higher hydrate does not affect any of the conclusions drawn below.

Although the identity of the non-cubic, hydrated form of the $NaCl_{(s)}$ particles is not fully understood, their ice nucleating ability can be probed and compared to $NaCl_{(s)}$. Figure 7 shows the results of a typical ice nucleating experiment on a sample containing both anhydrous and hydrated $NaCl_{(s)}$ particles. The mixed sample was created by deliquescing $NaCl_{(s)}$ particles and then efflorescing them at ~239 K. After efflorescence, particle temperature was decreased to 224 K while the RH in the environmental cell was maintained at RH values between 25 and 45 %. In this particular experiment, when the RH in the environmental cell was increased to ~63 % (at 224 K), ice began to nucleate on top of one of the hydrated particles. In order to confirm that ice was nucleating on a hydrated particle, Raman spectra were taken of the ice and the ice nuclei. The Raman spectrum (spectrum (a) in Fig. 7) had peaks indicative of a hydrated $NaCl_{(s)}$ particle and ice. After the ice was sublimed from the sample, a Raman spectrum was collected (spectrum (b) in Fig. 7) of the ice nuclei. This spectrum again confirmed that the ice nucleus was a hydrated particle. In this particular experiment, ice formed on the hydrated particles at S_{ice} of 1.01.

Several ice nucleation experiments were performed on mixed anhydrous and hydrated $NaCl_{(s)}$ samples at various temperatures. The results of these experiments are plotted in Fig. 8 in S_{ice}/temperature space. All S_{ice} data were put into bins that span two degrees Kelvin and averaged. Each data
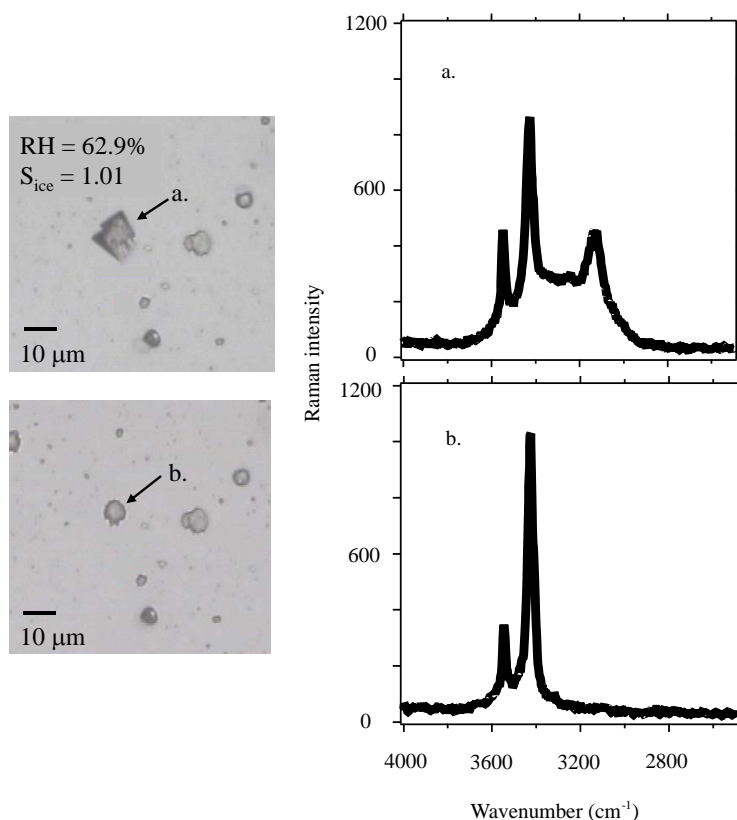
Fig. 7. Depositional ice nucleation experiment performed at 224 K on a mixed hydrated/anhydrous $NaCl_{(s)}$ sample. Particle **(a)** in the top left image is an ice particle which nucleated on a hydrated $NaCl_{(s)}$ particle at an S_{ice} value of 1.01. Particle **(b)** in the lower left image is the ice nucleus after the ice was sublimed. Raman spectra of both particles were taken to confirm the presence of ice and the hydrated $NaCl_{(s)}$ particle.

point represents the average S_{ice} value for each temperature bin. The error range (represented by the lines) is the high and low value for each bin. Additionally, the grey error bars represent the experimental error. Over the temperature range studied, it can be seen that the hydrated $NaCl_{(s)}$ particles nucleate ice at S_{ice} values between 0.98 and 1.06 (open circles in Fig. 8). Additionally, there does not appear to be a temperature or size dependence on the ice nucleating ability of hydrated $NaCl_{(s)}$ particles. This result is similar to Baustian et al. (2010). The average S_{ice} value for the 21 experiments is 1.02 ± 0.04.

Using the mixed samples, it was observed that the ice nucleated preferentially on the hydrated $NaCl_{(s)}$ particles over the anhydrous particles. In every case, the hydrated $NaCl_{(s)}$ particles nucleated ice before the anhydrous $NaCl_{(s)}$ particles. In order to confirm this observation, ice nucleation experiments were performed on samples containing only anhydrous $NaCl_{(s)}$ particles (filled squares in Fig. 8). Over the same temperature range, anhydrous $NaCl_{(s)}$ particles nucleated ice at S_{ice} values between 1.02 and 1.21. The average S_{ice} value for the 9 experiments performed on anhydrous

$NaCl_{(s)}$ particles is 1.11 ± 0.07. Student's t-test was performed with the binned anhydrous $NaCl_{(s)}$ and binned hydrated $NaCl_{(s)}$ S_{ice} data. For a two-tailed T-test, the P-value is 0.0012. Therefore, there is a statistical difference between the binned S_{ice} values for the anhydrous and hydrated $NaCl_{(s)}$ particles. Furthermore, ice nucleated preferentially on the hydrated $NaCl_{(s)}$ particles in the mixed samples.

In the above experiments, hydrated $NaCl_{(s)}$ particles were sometimes observed to undergo deliquescence and sometimes depositional ice nucleation occurred. To examine the two processes, the depositional ice nucleation and deliquescence data for the hydrated $NaCl_{(s)}$ particles are plotted in RH versus temperature space (Fig. 9).

Between 221 and 238 K, the RH at which depositional ice nucleation occurs on the hydrated particles increases from 62 to 79 % ($S_{ice} = 1$–1.11). Similarly, between 235 and 239 K, the RH at which deliquescence occurs increases from 77 to 93 % ($S_{ice} = 1.11$–1.30). In this temperature region (denoted with the gray shading) both deliquescence and depositional ice nucleation occurs. As the temperature is warmed from 239 K, only deliquescence occurs and the DRH decreases.
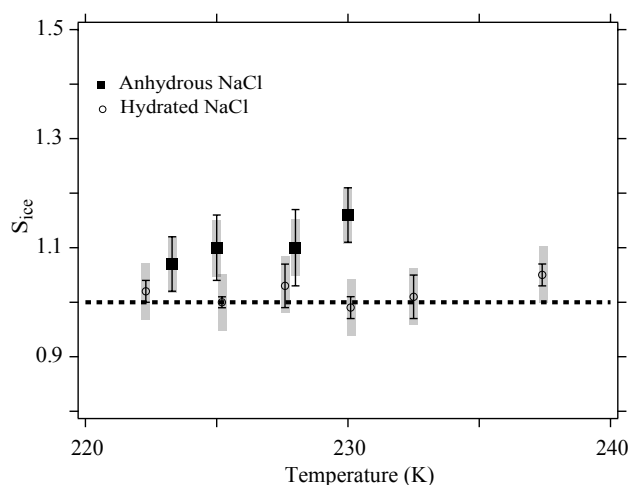
Fig. 8. S_{ice} versus temperature for the onset of depositional ice nucleation on NaCl (solid squares) and hydrated NaCl particles (open circles). An S_{ice} of 1 is denoted with the dotted line. Here, depositional ice nucleation is defined as the onset of ice nucleation and represents the conditions at which the first particle on the substrate nucleated ice. The error range (represented by the lines) is the high and low value for each bin. Additionally, the grey error bars represent experimnetal error.
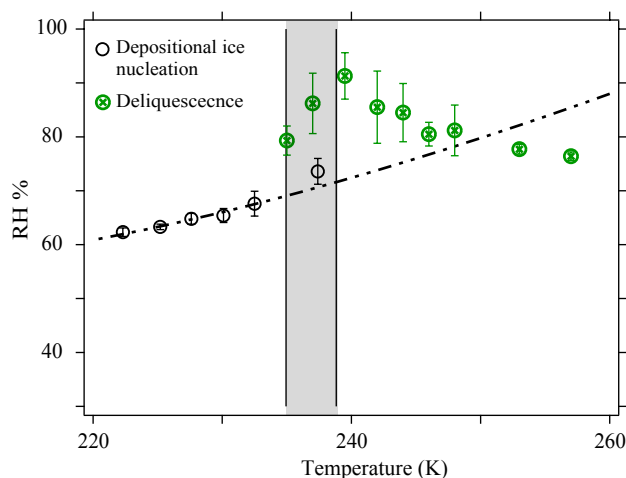

Fig. 9. Relative humidity versus temperature for depositional ice nucleation on hydrated NaCl$_{(s)}$ (open circles) and deliquescence of hydrated NaCl$_{(s)}$ (crossed green circles). The grey shading denotes the temperatures at which both depositional ice nucleation and deliquescence occur. The dashed-dotted line represents RH at an $S_{ice} = 1$.

The shapes of the depositional ice nucleation and deliquescence curves show that the data are consistent with one another. At temperatures warmer than 239 K, the particles will deliquesce and at temperatures below 235 K the particles will depositionally nucleate ice.

The hydrated NaCl$_{(s)}$ particles prepared in this study appear to have a rougher surface than that of the dehydrated NaCl$_{(s)}$ particles. This surface roughness might be one reason for the very low ice nucleation threshold for such particles. It has been shown previously that ammonium sulfate crystals can act as IN in an immersion ice nucleation process (Zuberi et al., 2001). In these experiments it was observed that crystals with a polycrystalline structure, i.e. a rougher surface, nucleated ice at very low supersaturation ($S_{ice} \sim 1.08$–1.18) while smooth single crystals required significant supersaturation ($S_{ice} \sim 1.64$–1.67).

It has been suggested that heterogeneous ice nucleation is initiated when an ice embryo forms at an ice-active surface site. Sullivan et al. (2010) tested this hypothesis by "processing" Arizona Test Dust with sulfuric acid. They found that the processed dust had a decreased ice nucleation efficiency compared to the unprocessed dust. This result was attributed to the acid digestion of ice surface sites. Although we do not have any direct evidence for hydrated NaCl$_{(s)}$ particles having more ice-active surface sites than dehydrated NaCl$_{(s)}$ particles, it is a plausible hypothesis given the morphology of the particles. Another plausible hypothesis is that the hydration waters may be good sites to adsorb further water and nucleate ice

4 Atmospheric implications

The results of this study show that the hydrated form of NaCl$_{(s)}$ is a very good IN. However, it is not known whether or not hydrated NaCl$_{(s)}$ is present enough of the time in the troposphere to affect ice nucleation. Therefore, the water uptake and depositional ice nucleation data collected in this study for NaCl$_{(s)}$ and hydrated NaCl$_{(s)}$ were used in a trajectory model following the approach used by Jensen et al. (2010).

The result of the model is shown graphically in Fig. 10. Specifically, the temperature, relative humidity, and NaCl phase was tracked along parcel trajectories after they were detrained from deep convection (at 100 % RH). (See Jensen et al., 2010 for details.) The particles were initially assumed to be aqueous NaCl with 100 % relative humidity with respect to ice. The RH in each parcel was tracked on its path upward through the tropical upper troposphere. If the RH dropped below 35 %, NaCl particles in the parcel were assumed to effloresce. They remained NaCl$_{(s)}$ unless the RH increased above the deliquescence point (80 %). By combining results from 648 trajectories throughout the tropics, statistics were generated of the time when NaCl particles were in aqueous or solid states. It was calculated, at temperatures below 220 K, that hydrated NaCl$_{(s)}$ is present 40–80 % of the time in the troposphere.

The lowest efflorescence temperature utilized in the laboratory studies presented in this manuscript was 239 K. Figure 10 shows a scenario that uses temperatures from

180–220 K. Thus a significant temperature extrapolation was assumed. This could introduce error in the model, especially at the lowest temperature. Between room temperature and 238 K, we did not observe significant temperature dependence in the ERH. Thus it is reasonable to assume a similar trend at lower temperatures.

In a similar study to model the deliquescence and efflorescence behavior of ammoniated sulfate particles, Colberg et al. (2003) assumed a constant offset between the DRH and ERH independently of temperature based on available data for ammonium sulfate. We note that if the DRH of the hydrated form of NaCl increases slightly with decreasing temperature similarly to that suggested for $NaCl \cdot 2H_2O_{(s)}$, one would expect an increasing ERH at the lowest temperatures. This would lead to a larger fraction of particles being in a hydrated crystalline form. Hence, our approach of a constant ERH is a conservative estimate of the fraction of crystalline particles.

Further, the values of S_{ice} did not change appreciably over the experimental temperature range down to 225 K. However, past work has shown that S_{ice} values do increase at temperatures below 180 K, (Trainer et al., 2009), so an extrapolation would be needed for cirrus at the very lowest temperatures in the atmosphere.

Because hydrated $NaCl_{(s)}$ particles could be frequently present, they could play a role in cirrus cloud formation. Cziczo et al. (2004) found that sea salt was often incorporated in anvil cirrus clouds formed near the Florida peninsula. They hypothesized that the ice crystals formed via a homogeneous nucleation mechanism. However, the current study suggests that a different pathway of ice formation for the anvil cirrus clouds is possible. If the temperature and RH conditions are right, hydrated $NaCl_{(s)}$ can compete with mineral dust for ice nucleation via a heterogeneous mechanism.

In addition to impacting atmospheric ice, hydrated $NaCl_{(s)}$ may also have a climatic impact. The ratio of the radiative forcing, ΔF_R, of the hydrated NaCl particles (denoted with a subscript "h") with respect to the anhydrous particles (denoted with a subscript "dry") is calculated using the equation

$$\Delta F_R = \frac{Q_{ext,h} D_h^2 (1 - g_h/2)}{Q_{ext,dry} D_{dry}^2 (1 - g_{dry}/2)} \tag{1}$$

where Q_{ext} is the extinction efficiency, D is the particle diameter, and g is the asymmetry parameter. This equation is valid for an optically thin, non-absorbing layer of aerosol particles in a clear sky (Chylek and Wong, 1995).

The raio of diameters for the hydrated to anhydrous NaCl was determined experimentally. The ratio of diameters is usually expressed as a growth factor, G_f,

$$G_f = \frac{D_h}{D_{dry}} \tag{2}$$

Using the optical microscope, anhydrous particle diameters were first measured. Then particles were deliquesced and
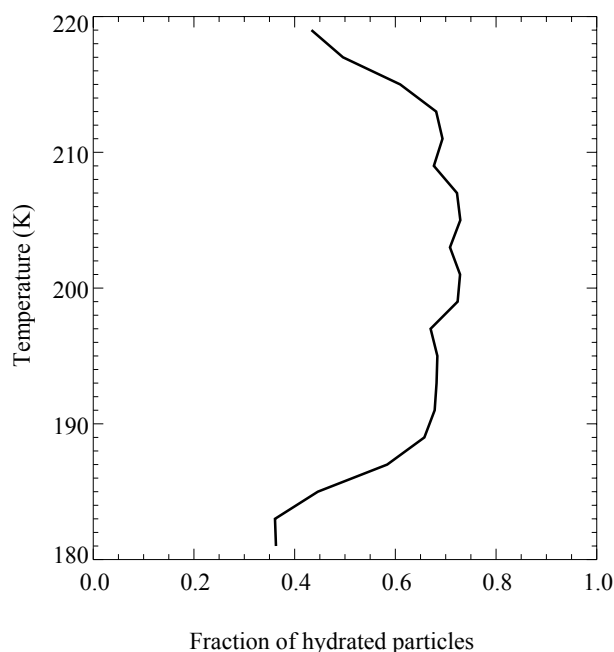

Fig. 10. Fraction of hydrated particles at temperatures ranging from 180 to 220 K.

their sizes measured, followed by efflorescence at temperatures between 239 and 249 K. Efflorescence resulted in hydrated particles. The same particles were thus measured in the dry, deliquesced and hydrated state and growth factors on a particle by particle basis were determined. Using a population of 93 particles, an average growth factor of 2.01 ± 0.22 was measured for the deliquesced particles at an average RH of 81.6 %. Using a population of 52 particles, an average growth factor of 1.46 ± 0.13 was measured for the hydrated $NaCl_{(s)}$ particles. The value obtained for aqueous NaCl is in agreement with the prediction from the E-AIM model of 1.98 at 81.6 % RH (Clegg et al., 1998, http://www.aim.env.uea.ac.uk/aim/aim.php). This gives us added confidence that the growth factor for the hydrated NaCl particles is a reasonable approximation.

To use Eq. (1) to determine the radiative forcing ratio, it is also necessary to estimate the extinction efficiencies and asymmetry parameters. Both of these values were calculated using MATLAB versions of Mie codes adapted from Bohren and Huffman (2004) and Mätzler (2002). To account for a range of different particle sizes, these values were calculated using particle diameters from 10 nm to 5.0 µm. Because the solar spectrum includes ultraviolet, visible, and infrared wavelengths, we have included wavelengths from 200 nm to 1.5 µm.

As input into the Mie calculations, the refractive indices of the dry and hydrated NaCl are needed. The literature values for the complex refractive index of $NaCl_{(s)}$ were obtained from Toon et al. (1976). The literature values for the complex

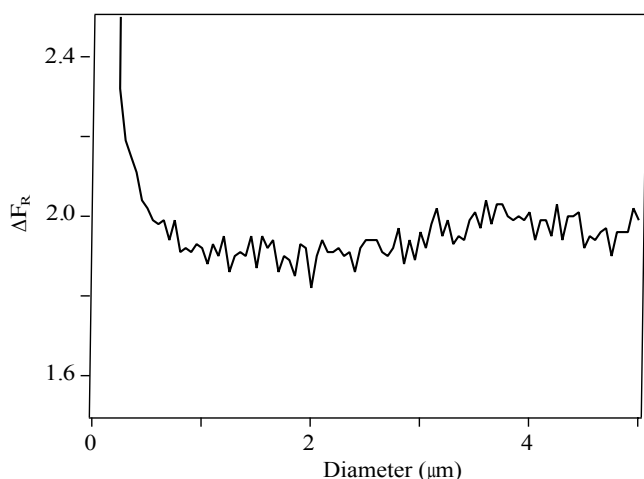**Fig. 11.** Ratio of the radiative forcing of hydrated NaCl particles with respect to dry particles (ΔF_R) as a function of particle diameter.

refractive index of water were obtained from Seinfeld and Pandis (2006). Refractive indices for $NaCl_{(s)}$ and water at wavelengths that were not available from these sources were linearly extrapolated over small wavelength ranges. Water has several absorption bands in the near infrared (Curcio and Petty, 1951). The real part of the refractive index has its greatest sensitivity to frequency around the absorption band (McHale, 1999). For the weaker water transitions in the near infrared, changes in the imaginary part of the refractive index cause little visible change in the real part of the refractive index (Ray, 1972; Huibers, 1997). We have capped the wavelength range for the calculation to $1.5\,\mu m$ to avoid the stronger absorption bands at $1.94\,\mu m$ and higher wavelengths (Curcio and Petty, 1951). The refractive index of the hydrate was calculated for each wavelength using the experimentally determined growth factor. The complex refractive index for the hydrate is given by

$$n_{NaCl_{(aq)}} = \frac{V_h - V_{dry}}{V_h} n_{H_2O} + \frac{V_{dry}}{V_h} n_{NaCl_{(s)}}$$
$$= \left(1 - G_f^{-3}\right) n_{H_2O} + G_f^{-3} n_{NaCl_{(s)}} \qquad (3)$$

where V_h and V_{dry} are the volumes of the hydrated and dry particles, respectively. ΔF_R was calculated using Eq. (1) for the hydrated relative to anhydrous NaCl particles (Fig. 11). The oscillations observed in Fig. 11 are caused by the oscillations observed in Mie scattering curves as a function of size parameter. Because the hydrated and anhydrous particles do not absorb over the wavelength range used in the calculation besides a few weak transitions of water in the near infrared, the particles scatter radiation. The value of ΔF_R observed over all sizes is greater than unity, indicating an enhancement in cooling for the hydrates. The enhancement is largest for the smallest particle sizes. The average ΔF_R for particles

500 nm in diameter and larger is 1.94 for hydrated $NaCl_{(s)}$ relative to $NaCl_{(s)}$. Thus neglect of hydration for NaCl particles could lead to a factor of two error in the calculated radiative forcing. It is important to note that ΔF_R is a ratio of two negative numbers. Therefore, the result is a positive number even though the particles do in fact lead to a cooling.

5 Conclusions

In this manuscript we have presented new laboratory experiments showing the formation of a NaCl hydrate upon efflorescence of small NaCl droplets at low temperatures. This hydrate is a better ice nucleus than dry NaCl particles as it does not require any significant supersaturation at temperatures below about 235 K. Model calculations of the potential occurrence of the hydrated NaCl particles in the upper troposphere together with radiative transfer calculations suggest a significant impact on the radiative forcing of such particles.

Edited by: M. Ammann

References

Baustian, K. J., Wise, M. E., and Tolbert, M. A.: Depositional ice nucleation on solid ammonium sulfate and glutaric acid particles, Atmos. Chem. Phys., 10, 2307–2317, doi:10.5194/acp-10-2307-2010, 2010.

Biskos, G., Malinowski, A., Russell, L. M., Buseck, P. R., and Martin, S. T.: Nanosize effect on the deliquescence and the efflorescence of sodium chloride particles, Aerosol Sci. Tech., 40, 97–106, 2006.

Bohren, C. F. H. and Huffman, D. R.: Absorption and scattering of light by small particles, Wiley-VCH, Weinheim, Germany, 2004.

American Chemical Society: Solubilities of Inorganic and Metal Organic Compounds, 4th edn., edited by: Linke, W. F., American Chemical Society, Washington DC, USA, 1965.

Chylek, P. and Wong, J.: Effect of absorbing aerosols on global radiation budget, Geophys. Res. Lett., 22, 8, 929–931, doi:10.1029/95GL00800, 1995.

Clegg, S. L., Brimblecombe, P., and Wexler, A. S.: A thermodynamic model of the system H^+-NH_4^+-Na^+-SO_4^{2-}-NO_3^--Cl^--H_2O at 298.15 K, J. Phys. Chem. A, 102, 2155–2171, 1998.

Colberg, C. A., Luo, B. P., Wernli, H., Koop, T., and Peter, Th.: A novel model to predict the physical state of atmospheric H_2SO_4/NH_3/H_2O aerosol particles, Atmos. Chem. Phys., 3, 909–924, doi:10.5194/acp-3-909-2003, 2003.

Curcio, J. A. and Petty, C. C.: The near infrared absorption spectrum of liquid water, J. Opt. Soc. Am., 41, 302–304, 1951.

Cziczo, D. J. and Abbatt, J. P. D.: Infrared observations of the response of NaCl, MgCl$_2$, NH$_4$HSO$_4$, and NH$_4$NO$_3$ aerosols to changes in relative humidity from 298 to 238 K, J. Phys. Chem. A, 104, 2038–2047, 2000.

Cziczo, D. J., Murphy, D. M., Hudson, P. K., and Thomson, D. S.: Single particle measurements of the chemical composition of cirrus ice residue during CRYSTAL-FACE, J. Geophys. Res., 109, D04201, doi:10.1029/2003jd004032, 2004.

De Haan, D. O. and Finlayson-Pitts, B. J.: Knudsen cell studies of the reaction of gaseous nitric acid with synthetic sea salt at 298 K, J. Phys. Chem. A, 101, 9993–9999, 1997.

Dubessy, J., Audeoud, D., Wilkins, R., and Kosztolanyi, C.: The use of the Raman micro-probe MOLE in the determination of the electrolytes dissolved in the aqueous phase of fluid inclusions, Chem. Geol., 37, 137–150, 1982.

Ewing, G. E.: H$_2$O on NaCl: From single molecule, to clusters, to monolayer, to thin film, to deliquescence, Struct. Bond., 116, 1–25, 2005.

Haywood, J. M., Ramaswamy, V., and Soden, B. J.: Tropospheric aerosol climate forcing in clear-sky satellite observations over the oceans, Science, 283, 1299–1303, 1999.

Jensen, E. J., Pfister, L., Bui, T.-P., Lawson, P., and Baumgardner, D.: Ice nucleation and cloud microphysical properties in tropical tropopause layer cirrus, Atmos. Chem. Phys., 10, 1369–1384, doi:10.5194/acp-10-1369-2010, 2010.

Huibers, P. D. T.: Models for the wavelength dependence of the index of refraction of water, Appl. Optics, 36, 3785–3787, 1997.

Koop, T., Kapilashrami, A., Molina, L. T., and Molina, M. J.: Phase transitions of sea-salt/water mixtures at low temperatures: Implications for ozone chemistry in the polar marine boundary layer, J. Geophys. Res., 105, 26393–26402, doi:10.1029/2000JD900413, 2000.

Koop, T.: Homogeneous ice nucleation in water and aqueous solutions, Z. Phys. Chem., 218, 1231–1258, 2004.

IAP Research Report, no. 2002-08: http://Diogenes.iwt.unibremen. de/vt/laser/wriedt/Mie_Type_Codes/body_mie_type_codes. html(available online), last access: May 2008, 2002.

Krepelova, A., Huthwelker, T., Bluhm, H., and Ammann, M.: Surface chemical properties of eutectic and frozen NaCl solutions probed by XPS and NEXAFS, Chem. Phys. Chem., 11, 3859–3866, 2010.

Kurtz, C. A. and Richardson, C. B.: Measurement of phase-changes in a microscopic lithium iodide particle levitated in water-vapor, Chem. Phys. Lett., 109, 190–194, 1984.

Lide, D. R.: CRC Handbook of Chemistry and Physics (Internet version 2011), 91 edn., CRC Press, Boca Raton, FL, 2011.

Linke, W. F. : Solubilities of Inorganic and Metal Organic Compounds, 4th edn., American Chemical Society, Washington DC, USA, 1965.

Martin, S. T.: Phase transitions of aqueous atmospheric particles, Chem. Rev., 100, 3403–3453, 2000.

Mätzler, C.: MATLAB Functions for Mie Scattering and Absorption, Version 2, IAP Research Report, no. 2002-11, Institut für angewandte Physik, Universität Bern, 2002.

McHale, J. L.: Molecular spectroscopy, Prentice-Hall, New Jersey, USA, 1999.

Middlebrook, A. M., Murphy, D. M., and Thomson, D. S.: Observations of organic material in individual marine particles at Cape Grim during the First Aerosol Characterization Experiment (ACE 1), J. Geophys. Res., 103, 16475–16483, doi:10.1029/97JD03719, 1998.

Mikhailov, E., Vlasenko, S., Martin, S. T., Koop, T., and Pöschl, U.: Amorphous and crystalline aerosol particles interacting with water vapor: conceptual framework and experimental evidence for restructuring, phase transitions and kinetic limitations, Atmos. Chem. Phys., 9, 9491–9522, doi:10.5194/acp-9-9491-2009, 2009.

O'Dowd, C. D., Facchini, M. C., Cavalli, F., Cebrunis, D., Mircea, M., Decesari, S., Fuzzi, S., Yoon, Y. J., and Putard, J. P.: Biogenically driven organic contribution to marine aerosol, Nature, 431, 676–680, 2004.

Pilson, M. E. Q.: An Introduction to the Chemistry of the Sea, Prentice Hall, Upper Saddle River, NJ, 1998.

Ray, P. S.: Broadband complex refractive indices of ice and water, Appl. Optics, 11, 1836–1844, 1972.

Seinfeld, J. H. and Pandis, S. N.: Atmospheric chemistry and physics: From air pollution to climate change, 2nd edn., Wiley, New Jersey, USA, 2006.

Tang, I. N., Munkelwitz, H. R., and Davis, J. G.: Aerosol growth studies – II. Preparation and growth measurements of monodisperse salt aerosols, J. Aerosol Sci., 8, 149–159, 1977.

Tang, I. N. and Munkelwitz, H. R.: Composition and temperature dependence of the deliquescence properties of hygroscopic aerosols, Atmos. Environ., 27A, 467-473, 1993.

Tang, I. N., Tridico, A. C., and Fung, K. H.: Thermodynamic and optical properties of sea salt aerosols, J. Geophys. Res., 102, 23,269–23,275, doi:10.1029/96JD03085, 1997.

Textor, C., Schulz, M., Guibert, S., Kinne, S., Balkanski, Y., Bauer, S., Berntsen, T., Berglen, T., Boucher, O., Chin, M., Dentener, F., Diehl, T., Easter, R., Feichter, H., Fillmore, D., Ghan, S., Ginoux, P., Gong, S., Grini, A., Hendricks, J., Horowitz, L., Huang, P., Isaksen, I., Iversen, I., Kloster, S., Koch, D., Kirkevåg, A., Kristjansson, J. E., Krol, M., Lauer, A., Lamarque, J. F., Liu, X., Montanaro, V., Myhre, G., Penner, J., Pitari, G., Reddy, S., Seland, Ø., Stier, P., Takemura, T., and Tie, X.: Analysis and quantification of the diversities of aerosol life cycles within AeroCom, Atmos. Chem. Phys., 6, 1777–1813, doi:10.5194/acp-6-1777-2006, 2006.

Toon, O. B., Pollack, J. B., and Khare, B. N.: The optical constants of several atmospheric aerosol species: Ammonium sulfate, aluminum oxide, and sodium chloride, J. Geophys. Res, 81, 5733–5748, 1976.

Trainer, M. G., Toon, O. B., and Tolbert, M. A.: Measurements of depositional ice nucleation on insoluble substrates at low temperatures: Implications for Earth and Mars, J. Phys, Chem. C, 113, 2036–2040, 2009.

Vinoj, V. and Satheesh, S. K.: Measurements of aerosol optical depth over Arabian Sea during summer monsoon season, Geophys. Res. Lett., 30, 1263, doi:10.1029/2002GL016664, 2003.

Wise, M. E., Biskos, G., Martin, S. T., Russell, L. M., and Buseck, P. R.: Phase transitions of single salt particles studied using a transmission electron microscope with an environmental cell, Aerosol Sci. Tech., 39, 849–856, 2005.

Wise, M. E., Martin, S. T., Russell, L. M., and Buseck, P. R.: Water uptake by NaCl particles prior to deliquescence and the phase rule, Aerosol Sci. Tech., 42, 281–294 2008.

Wise, M. E., Baustian, K. J., and Tolbert, M. A.: Internally mixed sulfate and organic particles as potential ice nuclei in the tropical tropopause region, P. Natl. Acad. Sci. USA, 107, 6693–6698, doi:10.1073/pnas.0913018107, 2010.

Zuberi, B., Bertram, A. K., Koop, T., Molina, L. T., and Molina, M. J.: Heterogeneous freezing of aqueous particles induced by crystallized $(NH_4)_2SO_4$, ice and letovicite, J. Phys Chem. A, 105, 26, 6458–6464, 2001.